Journal of Mechanical Design

Technical Briefs

A Pseudo-Rigid-Body Model for Initially-Curved Pinned-Pinned Segments Used in Compliant Mechanisms

Brian T. Edwards,[1] Brian D. Jensen,[2] and Larry L. Howell
Mechanical Engineering Department, Brigham Young University, Provo, UT 84602

The pseudo-rigid-body model concept allows compliant mechanisms to be analyzed using well-known rigid-body kinematics. This paper presents a pseudo-rigid-body model for initially curved pinned-pinned segments that undergo large, nonlinear deflections. The model approximates the segment as three rigid members joined by pin joints. Torsional springs placed at the joints model the segment's stiffness. This model has been validated by fabricating several such segments from a variety of different materials. Testing of the force-deflection behavior of these segments verified the accuracy of the model.
[DOI: 10.1115/1.1376396]

Introduction

The nonlinear deflections often associated with the motion of compliant mechanisms increase the complexity of compliant mechanism analysis and design. However, these deflections allow a drastic reduction in part count, increase in reliability, and all of the other advantages of compliant mechanisms [1,2]. Methods must be developed that simplify large-deflection analysis to aid in compliant mechanism design. The pseudo-rigid-body model concept has been developed in response to this need [3]. This model unifies compliant mechanism theory with rigid-body mechanism theory by replacing a compliant segment with two or more rigid segments joined by pin joints. The lengths of the equivalent rigid segments are specified so that their motion closely models that of the compliant segments. A torsional spring at the pin joint models the segment's resistance to bending. This type of model has been applied to small-length flexural pivots [3], initially straight fixed compliant segments with external end loads [4], and initially curved segments with similar loads [5].

A common compliant link yet to be modeled is the initially-curved pinned-pinned segment, or functionally binary pinned-pinned segment (FBPP), shown in Fig. 1 [6]. Because it is pinned at both ends, vertical loads cause rigid-body rotation; only horizontal loading produces deflection. Thus, the segment behaves much like a translational spring. However, its force-deflection characteristics are not linear. To better study these characteristics, symmetry is used to divide the complete segment into two equivalent half-segments, shown in Fig. 2. This half-segment will be modeled, and the results will be generalized to the full FBPP segment.

Elliptic Integral Solution

The force-deflection relationships for FBPP segments require a nonlinear solution. The classical method for determining these relationships has been through elliptic integrals [7,8]. For a fixed-pinned curved beam with a horizontal force applied to the pinned end, the solutions are [9]:

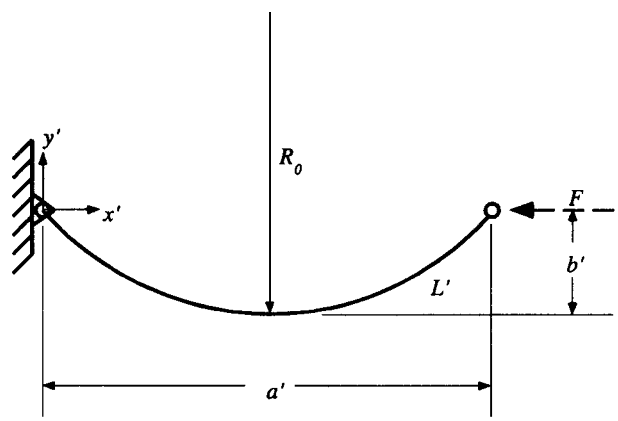

Fig. 1 A functionally binary pinned-pinned (FBPP) segment

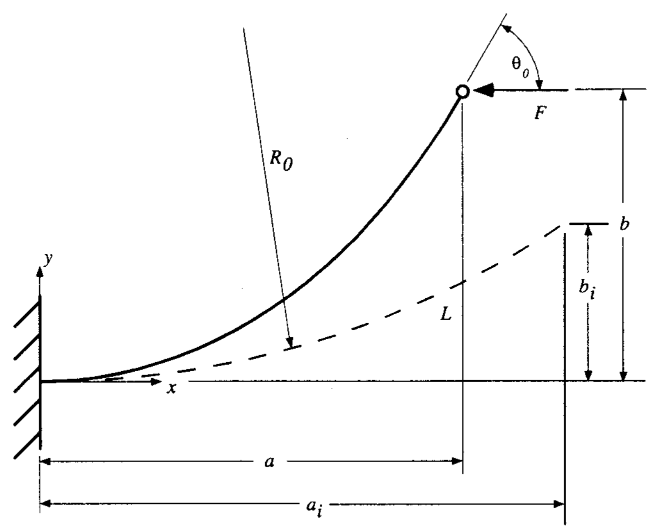

Fig. 2 Half-model of FBPP segment

[1]Currently at Mechanical Dynamics Inc., Ann Arbor, Michigan
[2]Currently at the University of Michigan, Ann Arbor, Michigan

Contributed by the Design for manufacturability Committee for publication in the JOURNAL OF MECHANICAL DESIGN. Manuscript received June 1999. Associate Technical Editor: S. Kota.

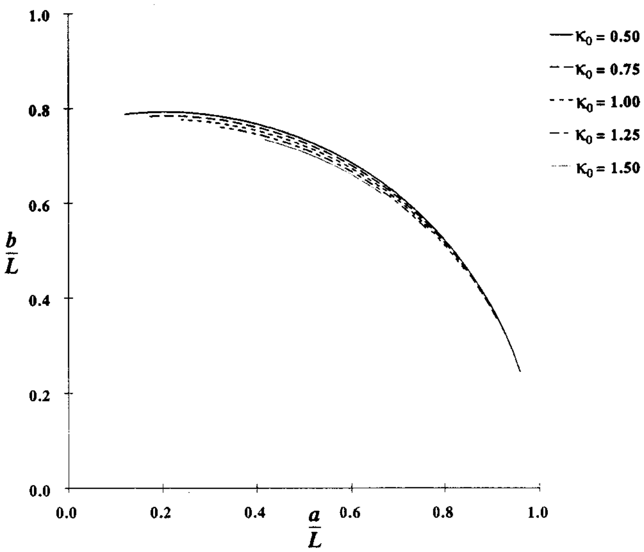

Fig. 3 Non-dimensionalized tip deflection at various κ_0 values

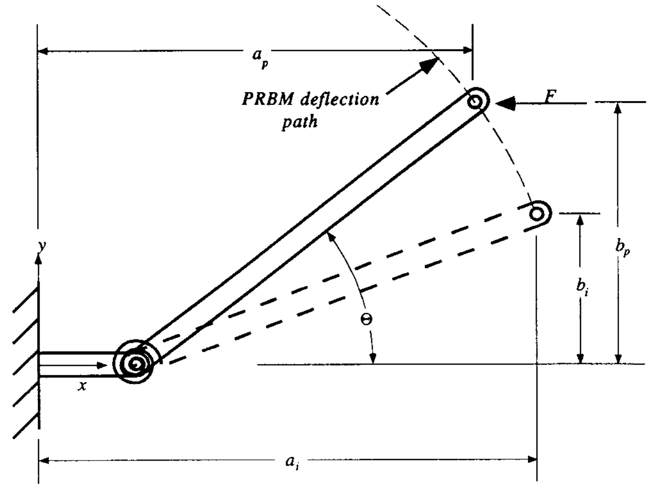

Fig. 4 PRBM in deflected position

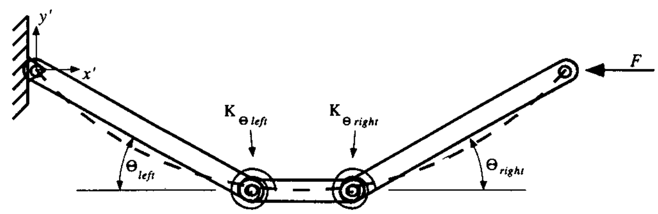

Fig. 5 PRBM for entire FBPP segment

For $\lambda > 1$

$$\frac{a}{L} = \frac{1}{\alpha t}[(t^2 - 2)F(\beta,t) + 2E(\beta,t)] \tag{1}$$

$$\alpha = tF(\beta,t) \tag{2}$$

where

$$\alpha^2 = \frac{FL^2}{EI} \tag{3}$$

$$\lambda = \frac{\kappa_0^2}{2\alpha^2} - \cos\theta_0 \tag{4}$$

$$\kappa_0 = \frac{L}{R_0} \tag{5}$$

$$\beta = \frac{\theta_0}{2} \tag{6}$$

$$t = \sqrt{\frac{2}{\lambda + 1}} \tag{7}$$

Also, R_0 is the initial radius of curvature of the segment, L is the segment length, θ_0 is the angle the pinned end of the deflected beam makes with the x-axis, and a is the x-coordinate of the pinned end, measured from the fixed end of the beam. EI is the beam's flexural rigidity, and F is the applied horizontal force. $F(\beta,t)$ is the incomplete elliptic integral of the first kind, and $E(\beta,t)$ is the incomplete elliptic integral of the second kind. For Eqs. (1) and (2),

$$0 < \theta_0 \leq \pi \tag{8}$$

Similarly, for $|\lambda| < 1$,

$$\frac{a}{L} = \frac{1}{\alpha}[2E(\psi,r) - F(\psi,r)] \tag{9}$$

$$\alpha = F(\psi,r) \tag{10}$$

where

$$\psi = \operatorname{asin}\sqrt{\frac{1 - \cos\theta_0}{\lambda + 1}} \tag{11}$$

$$r = \sqrt{\frac{\lambda + 1}{2}} \tag{12}$$

and all other parameters are as defined previously. Finally, regardless of whether or not $\lambda > 1$,

$$\frac{b}{L} = \frac{\sqrt{2}}{\alpha}(\sqrt{\lambda + 1} - \sqrt{\lambda + \cos\theta_0}) \tag{13}$$

where b is the y-coordinate of the pinned end of the beam, measured from the fixed end.

Figure 3 presents the deflection characteristics for the beam tip at various values of κ_0, calculated using the elliptic integral solutions. Just as in previous studies for other beam loadings, the deflection curves for this type of beam loading are nearly circular, although not about the origin [4,5]. Therefore, the beam deflection can be modeled with an appropriately-placed pin joint and link.

The Pseudo-Rigid-Body Model

Using this concept, a simplified model, called the pseudo-rigid-body model (PRBM), can be developed to facilitate the force-deflection calculations for FBPP segments. This model, shown in Fig. 4, uses two rigid links and a torsional spring to approximate the nonlinear bending characteristics of the FBPP half-segment, with the link lengths and spring constant dependent on the initial geometry of the segment.

Note that, due to symmetry, the half-model is equally applicable to either side of the FBPP segment. Thus the entire FBPP segment shown in Fig. 1 may be represented in terms of an identical PRBM on each side of the segment midpoint. The resulting pseudo-rigid-body model is given in Fig. 5. The left and right sides are coupled by requiring the two angles Θ_{left} and Θ_{right} to be equal, as well as the torsional spring constants $K_{\Theta left}$ and $K_{\Theta right}$.

The model for fixed-free curved segments [5] is conceptually similar to the model in Fig. 4, thus allowing the pseudo-rigid-body model for the pinned-pinned segment to use some of the results developed for that model. But there are also significant differences that cause the two models to be different. One of the main differences is that the initially curved model is for combined vertical and horizontal forces on a cantilever beam. That model was based on the ratio of the horizontal to vertical force, which ratio would be infinity for the type of loading required in this paper. Another difference is that the elements are in series to accurately model the segment.

Derivation of the PRBM Link Lengths

For the PRBM in Fig. 4, it is apparent that the key factor governing accurate endpoint deflection approximations is obtaining the correct lengths for the two rigid links. The length of the fixed link is defined by the non-dimensionalized parameter γ, the ''fundamental radius factor,'' as $L(1-\gamma)$, where L is the length of the half-segment. The length of the second link must be the radius of the circular motion path described in Fig. 3. A parameter ρ is defined as the ''characteristic radius factor,'' with the distance ρL being the characteristic radius, after Howell and Midha [5] ρ is defined from geometry as

$$\rho=\sqrt{\left(\frac{a_i}{L}-(1-\gamma)\right)^2+\left(\frac{b_i}{L}\right)^2} \tag{14}$$

where a_i and b_i are the initial horizontal and vertical positions of the segment endpoint.

Since the initial locations of both the half-segment and PRBM endpoints are the same, the non-dimensionalized initial horizontal position, a_i/L, can be determined from known values as

$$\frac{a_i}{L}=\frac{1}{\kappa_0}\sin\kappa_0 \tag{15}$$

Similarly, the non-dimensionalized initial vertical endpoint position b_i/L is

$$\frac{b_i}{L}=\frac{1}{\kappa_0}(1-\cos\kappa_0) \tag{16}$$

Since the segment is initially curved, the angle the second link makes with the *x*-axis will be non-zero. This angle Θ, called the pseudo-rigid-body angle, has an initial value Θ_i of

$$\Theta_i=\tan^{-1}\left(\frac{b_i}{a_i-L(1-\gamma)}\right) \tag{17}$$

Upon application of a force F, the PRBM deflects to the position shown in Fig. 4. The new value of Θ is given by

$$\Theta=\tan^{-1}\left(\frac{b_p}{a_p-L(1-\gamma)}\right) \tag{18}$$

with a_p and b_p being the new horizontal and vertical coordinates of the PRBM endpoint. On the other hand, if Θ is known, the a_p and b_p may be found from

$$\frac{a_p}{L}=1-\gamma+\rho\cos\Theta \tag{19}$$

and

$$\frac{b_p}{L}=\rho\sin\Theta \tag{20}$$

Upon deflection, the PRBM endpoint path should stay within a specified error region (compared to the actual endpoint path) over a certain range of deflection. Thus the optimal PRBM is the one whose link lengths allow the largest range of deflection over which the error stays within the specified region. Because the fundamental radius factor, γ, determines the characteristic radius factor ρ, the deflection path depends only on γ. The solution method followed for obtaining the value of γ will be similar to that followed by Howell and Midha [5].

Table 1 PRBM rigid link characteristics

κ_0	γ	ρ	$(\Delta\Theta)_{max}$
0.50	0.793	0.791	1.677
0.75	0.787	0.783	1.456
1.00	0.783	0.775	1.327
1.25	0.779	0.768	1.203
1.50	0.775	0.760	1.070

At any two corresponding points on the PRBM and elliptic integral deflection curves, the relative error between the two paths is ε, where ε is defined to be

$$\varepsilon=\frac{\sqrt{(a-a_p)^2+(b-b_p)^2}}{\sqrt{(a-a_i)^2+(b-b_i)^2}} \tag{21}$$

The error region is defined as a non-dimensionalized constant distance ε_{max} on either side of the PRBM deflection path. The error region is narrow near the undeflected initial position, and widens as the angle of deflection increases. Finally, a variable $(\Delta\Theta)_{max}$ is defined as

$$(\Delta\Theta)_{max}=\Theta_{max}-\Theta_i \tag{22}$$

where Θ_{max} is the value of the pseudo-rigid-body angle at which the PRBM approximation exceeds the error bound ε_{max} $\cdot(\Delta\Theta)_{max}$ is then the difference between the initial angle of the rigid link and the final angle at which the error is exceeded.

The search for the optimal fundamental radius factor as a function of κ_0 then resolves into the following problem:

Find the value of γ which maximizes deflection angle $(\Delta\Theta)_{max}$, where

$$\varepsilon\leqslant\varepsilon_{max}\quad\text{for }\Theta_i\leqslant\Theta\leqslant\Theta_{max} \tag{23}$$

The optimization method implemented for finding γ is the Golden Section method [10]. For all cases, a parameter value of $\varepsilon_{max}=0.5$ percent was utilized. Table 1 shows the γ and ρ values at selected κ_0 values, with the corresponding $(\Delta\Theta)_{max}$ value for each curvature κ_0.

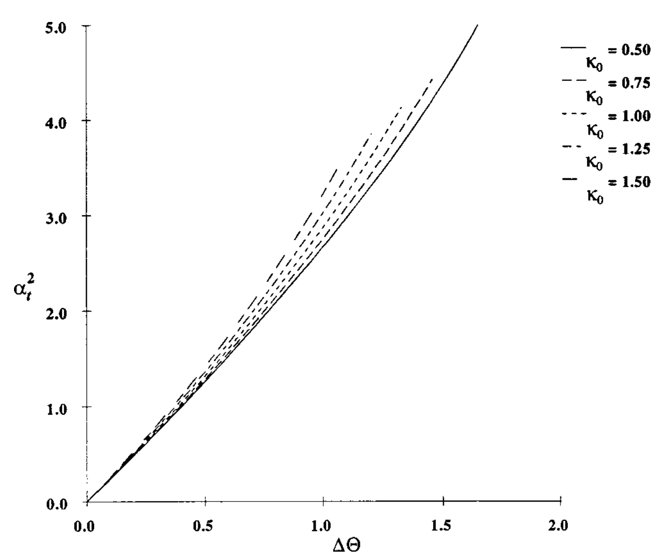

Fig. 6 Force-deflection relationship at various κ_0

Table 2 Torsional spring constant characteristics

κ_0	K_Θ	$(\Delta\Theta)_{max}$
0.50	2.59	0.99
0.75	2.62	0.86
1.00	2.68	0.79
1.25	2.75	0.71
1.50	2.83	0.63

Table 3 Second-order spring constant characteristics

κ_0	$K_{\Theta 1}$	$K_{\Theta 2}$	$(\Delta\Theta)_{max}$
0.50	2.24	0.46	1.68
0.75	2.30	0.48	1.46
1.00	2.34	0.55	1.33
1.25	2.40	0.64	1.20
1.50	2.48	0.73	1.07

The $\kappa_0-\gamma$ graph has two nearly linear regions along the curvature range. Hence two linear least-squares curve fits describing γ in terms of κ_0 are

$$\gamma = 0.8063 - 0.0265\kappa_0 \quad 0.500 \leqslant \kappa_0 \leqslant 0.595 \tag{24}$$

$$\gamma = 0.8005 - 0.0173\kappa_0 \quad 0.595 \leqslant \kappa_0 \leqslant 1.500 \tag{25}$$

with a correlation coefficient $r^2 \geqslant 0.999$ in each case.

Derivation of the PRBM Spring Constant

The spring constant of the torsional spring needs to be ascertained to complete the modeling of the segment's stiffness. Norton [11] and Howell et al. [12] proposed stiffness coefficients for initially straight fixed-pinned segments, while Howell and Midha [5] extended the theory to initially curved fixed-pinned segments subjected to variable-angle end forces. However, the case of pure horizontal loading has not been addressed by these authors. Because load direction strongly influences the equivalent spring stiffness [5], the modeling must be extended to predict FBPP segment deflection with sufficient accuracy.

Conceptually, the force component acting tangential to the link's motion, F_t, deflects the link, while the axial component F_a has no effect on rotation. The tangential force is

$$F_t = F \sin\Theta \tag{26}$$

The non-dimensionalized tangential force α_t^2 is then given by

$$\alpha_t^2 = \frac{FL^2 \sin\Theta}{EI} = \alpha^2 \sin\Theta \tag{27}$$

The deflection of the rigid link, $\Delta\Theta$, can be defined as the difference between the current pseudo-rigid-body angle and the initial angle, or

$$\Delta\Theta = \Theta - \Theta_i \tag{28}$$

For various non-dimensionalized curvatures κ_0, a graphical representation of the force-rotation deflection $(\alpha_t^2 - \Delta\Theta)$ relationship, based on the elliptic integral solutions, is found in Fig. 6. Over the first portion of the graph, the slope of each of the curves is nearly constant. Therefore, it may be modeled by a linear relationship as

$$\alpha_t^2 = K_\Theta \Delta\Theta \tag{29}$$

where K_Θ is the spring stiffness coefficient.

The approximation was extended over the largest $\Delta\Theta$ range possible while keeping the correlation coefficient $r^2 \geqslant 0.999$. Table 2 contains the values of K_Θ for selected curvatures κ_0.

If a simple equation is desired for quick calculations, the following relationship has a correlation coefficient $r^2 \geqslant 0.999$ and can be used to approximate the torsional spring constant for curvatures of $0.5 \leqslant \kappa_0 \leqslant 1.5$:

$$K_\Theta = 2.568 - 0.028\kappa_0 + 0.137\kappa_0^2 \tag{30}$$

The value of the torsional spring constant K may be found using the equation

$$K = \rho K_\Theta \frac{EI}{L} \tag{31}$$

When a larger $\Delta\Theta$ range is required, a second-order curve fit will accurately model the force-rotation relationship over the entire range that the PRBM deflection path is accurate. Similar to Eq. (29), it will be of the form

$$\alpha_t^2 = K_{\Theta 1}\Delta\Theta + K_{\Theta 2}(\Delta\Theta)^2 \tag{32}$$

The values for $K_{\Theta 1}$ and $K_{\Theta 2}$ at various curvatures are shown in Table 3. The equation for the spring function $K(\Delta\Theta)$ may be found using the approach used above for the first-order curve fit. It is

$$K(\Delta\Theta) = \rho \frac{EI}{L}(K_{\Theta 1} + K_{\Theta 2}\Delta\Theta) \tag{33}$$

Validation of the PRBM

To verify the PRBM for FBPP segments, several complete FBPP segments were machined for testing. Test mechanisms were created from A36-mild steel, 6061-T651 aluminum, and polypropylene, with the flexural rigidities (EI) being different in each case. Space does not allow the results to be reported in detail, but they are recorded in [6]. The plot of the deflection paths shows a close approximation of the PRBM equations to the actual physical segments, while more error is evident in the force-deflection curves. The selection of γ, which determines link lengths and deflection paths, requires deviation from the analytical solution of less than 0.5 percent. However, no strict bound is placed on the error implicit in choosing K_Θ; as a result, the model approximates actual behavior well but without the same accuracy expected for deflection predictions.

Conclusion

Functionally binary pinned-pinned segments are becoming important parts of many compliant mechanisms. Their non-linear deflection behavior, however, has complicated design. Therefore, FBPP segments have been analyzed in this paper to model their force-deflection characteristics. Elliptic integral solutions were used to develop analytic expressions for FBPP segment motion. Using these solutions, a pseudo-rigid-body model was developed to allow easier modeling of FBPP segments. This model represents the FBPP half-segment as two rigid beams joined by a pin joint. A torsional spring at the pin joint models segment stiffness. The force-deflection characteristics of the segment are modeled by choosing appropriate link lengths as well as the torsional spring constant. The accuracy of the model was tested using physical segments fabricated from aluminum, steel, and polypropylene. In each case, the model accurately predicted the segments' force-deflection characteristics.

Acknowledgments

This material is based upon work supported under a National Science Foundation Graduate Fellowship and a National Science Foundation Career Award No. DMI-9624574.

References

[1] Shoup, T. E., and McLarnan, C. W., 1971, ''A Survey of Flexible Link Mechanisms Having Lower Pairs,'' J. Mec., **6**, No. 3, pp. 97–105.
[2] Ananthasuresh, G. K., and Kota, S., 1995, ''Designing Compliant Mechanisms,'' Mech. Eng. (Am. Soc. Mech. Eng.), **117**, No. 11, pp. 93–96.
[3] Howell, L. L., and Midha, A., 1994, ''A Method for the Design of Compliant Mechanisms with Small-Length Flexural Pivots,'' ASME J. Mech. Des., **116**, No. 1, pp. 280–290.
[4] Howell, L. L., and Midha, A., 1995, ''Parametric Deflection Approximations for End-Loaded, Large-Deflection Beams in Compliant Mechanisms,'' ASME J. Mech. Des., **117**, No. 1, pp. 156–165.
[5] Howell, L. L., and Midha, A., 1996, ''Parametric Deflection Approximations for Initially Curved, Large-Deflection Beams in Compliant Mechanisms,'' *Proceedings of the 1996 ASME Design Engineering Technical Conferences*, 96-DETC/MECH-1215.
[6] Edwards, B. T., 1996, ''Functionally Binary Pinned-Pinned Segments,'' MS Thesis, Brigham Young University, Provo, UT.
[7] Bisshopp, K. E., and Drucker, D. C., 1945, ''Large Deflection of Cantilever Beams,'' Q. Appl. Math., **3**, No. 3, pp. 272–275.
[8] Frisch-Fay, R., 1962, *Flexible Bars*, Butterworth, Washington, D.C.
[9] Edwards, B. T., Jensen, B. D., and Howell, L. L., 1999, ''A Pseudo-Rigid-Body Model for Functionally Binary Pinned-Pinned Segments Used in Compliant Mechanisms,'' *Proceedings of the 1999 Design Engineering Technical Conferences*, DETC99/DAC-8644.
[10] Rao, S. S., 1984, *Optimization: Theory and Applications*, Wiley Eastern Limited, New Delhi.
[11] Norton, T. W., 1991, ''On the Nomenclature and Classification, and Mobility of Compliant Mechanisms,'' M.S. Thesis, Purdue University, West Lafayette, Indiana.
[12] Howell, L. L., Midha, A., and Norton, T. W., 1996, ''Evaluation of Equivalent Spring Stiffness for Use in a Pseudo-Rigid-Body Model of Large-Deflection Compliant Mechanisms,'' ASME J. Mech. Des., **118**, No. 1, pp. 126–131.

A Special Type of Crank Mechanism With Variable Stroke

Giovanni Mimmi
Dipartimento di Meccanica Strutturale, Università degli studi di Pavia, Via Ferrata, 1, I-27100 Pavia, Italy
e-mail: mimmi@unipv.it

Paolo Pennacchi
Dipartimento di Meccanica, Politecnico di Milano, Via La Masa, 34, I-20158 Milano, Italy
e-mail: paolo.pennacchi@polimi.it

The aim of this paper is a detailed analysis of a particular mechanism with variable piston stroke. This crank mechanism is presently applied to metering pumps, because it allows the piston stroke to be adjusted in length and permits the pump flow to be changed also during the pump functioning. The following analysis shows the different characteristics of piston motions obtainable by changing the ratios among the mechanism rod lengths.
[DOI: 10.1115/1.1376397]

Introduction

The mechanism that is the object of this paper is presently applied to diaphragm metering pumps: these pumps are used to meter and pump limited quantities of reagents in chemical industrial processes. In this case both the metering stoichiometric precision and also the timing of this operation are important. Then, the possibility offered by the studied crank gear of changing the piston stroke also during the pump functioning, illustrated in [1–4], results of great importance for this type of application.

In Fig. 1 a 3D representation of the mechanism is shown, while in Fig. 2 a simplified scheme is illustrated, which shows the kinematic constitutive components.

The functioning principle can be described as follows: the driving shaft C (element ❷ of Fig. 1) guides the rod BO to rotate (bush ❶ of Fig. 1). This rod is constrained by the crank AB in joint B (elements ❺ and ❹ of Fig. 1) and by the sliding-shoe in C; the result is a plane motion of the rod BO, in which the point B describes a circumference centered in A. This determines the motion of the connecting rod OD (element ❸ of Fig. 1); then, the piston D slides along the x axis. The length of the stroke of point D is analyzed as a function of the configuration system and, in particular, of the adjustable distance d (the length AC is adjustable and it allows to change the piston stroke).

Analytical Study of the Piston Motion

To obtain an analytical solution for the problem, it is necessary to calculate the expression of the angle α in Fig. 2 as a function of the drive shaft rotation ωt.

For this reason, the following equations system must be formulated:

$$\begin{cases} a^2+d^2-2ad\cos\alpha(t)=e^2(t) \\ a\cos\alpha(t)-e(t)\cos\omega t=d \end{cases} \tag{1}$$

that gives the solution:

$$e(t)=-d\cos\omega t+\sqrt{d^2\cos^2\omega t-d^2+a^2} \tag{2}$$

$$\cos\alpha(t)=\frac{d+e(t)\cos\omega t}{a} \tag{3}$$

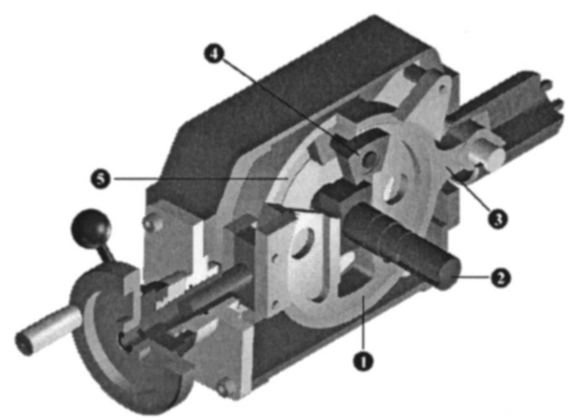

Fig. 1 3D representation of the studied mechanism

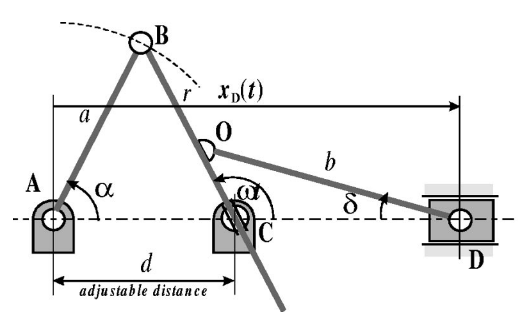

Fig. 2 Kinematic scheme of the mechanism

Contributed by the Design for Manufacturability Committee for publication in the JOURNAL OF MECHANICAL DESIGN. Manuscript received Oct. 1999. Associate Technical Editor: S. Kota .

The position of point D, referred to point A in the reference system of Fig. 2, can be expressed as:

$$x_D(t) = a\cos\alpha(t) - r\cos\omega t + b\cos\delta(t) \tag{4}$$

Because of $f(t)=e(t)-r$, the relation that connects ωt and $\delta(t)$ is immediately obtainable by the following relationship:

$$\frac{b}{\sin\omega t} = \frac{f(t)}{\sin\delta(t)} \tag{5}$$

from which:

$$\sin\delta(t) = \frac{f(t)}{b}\sin\omega t \tag{6}$$

By replacing the expressions (2), (3) and (6) into the (4) and by suitably rearranging the different terms, it results:

$$\begin{aligned} x_D(t) &= d + \cos\omega t\left(-d\cos\omega t + \sqrt{d^2(\cos^2\omega t - 1) + a^2}\right) - r\cos\omega t + b \\ &\quad \cdot \sqrt{1 - \left(\frac{-d\cos\omega t + \sqrt{d^2(\cos^2\omega t - 1) + a^2} - r}{b}\sin\omega t\right)^2} \end{aligned} \tag{7}$$

In order to obtain a real value of $x_D(t)$ from the Eq. (7), some conditions are needed that constrain the design parameters: in particular, for each value of time t, it must result:

$$d^2(\cos^2\omega t - 1) + a^2 \geqslant 0 \quad \forall t \Rightarrow AC \leqslant AB \tag{8}$$

$$|f(t)\sin\omega t| \leqslant b \quad \forall t \Rightarrow OC \leqslant OD \tag{9}$$

The last conditions require Eqs. (2) and (6) to have real solutions.

To proceed further in the analysis, it is advisable to make the function (7) non-dimensional by dividing $x_D(t)$ by the length of the rod AB, chosen as reference:

$$\begin{aligned} \tau_D(t) &= \tau_{d/a} + \cos\omega t\left(-\tau_{d/a}\cos\omega t + \sqrt{\tau_{d/a}^2(\cos^2\omega t - 1) + 1}\right) - \tau_{r/a}\cos\omega t \\ &\quad + \tau_{b/a} \cdot \sqrt{1 - \left(\frac{-\tau_{d/a}\cos\omega t + \sqrt{\tau_{d/a}^2(\cos^2\omega t - 1) + 1} - \tau_{r/a}}{\tau_{b/a}}\sin\omega t\right)^2} \end{aligned} \tag{10}$$

The piston stroke c is estimated as the difference between the maximum and the minimum value assumed by expression (7).

Piston Stroke Description

If the function (10) is represented for each value of time t (or, similarly, for each value of the drive shaft rotation angle ωt) and of the adjustable distance d, for a general set of rod lengths, the surface assumes the aspect shown in Fig. 3.

First of all, it is possible to observe that the surface is symmetric as regards time axis origin, because the functions $\cos\omega t$ e $\sin^2\omega t$ that appear in Eq. (10) are even functions. Further, the system behavior changes when the parameter $\tau_{d/a}$ increases:

- if $\tau_{d/a} < \tau^*_{d/a}$, the piston D runs only one stroke for each drive shaft rotation;
- if $\tau_{d/a} > \tau^*_{d/a}$, the piston D runs two strokes for each drive shaft rotation, but one of these strokes is incomplete.

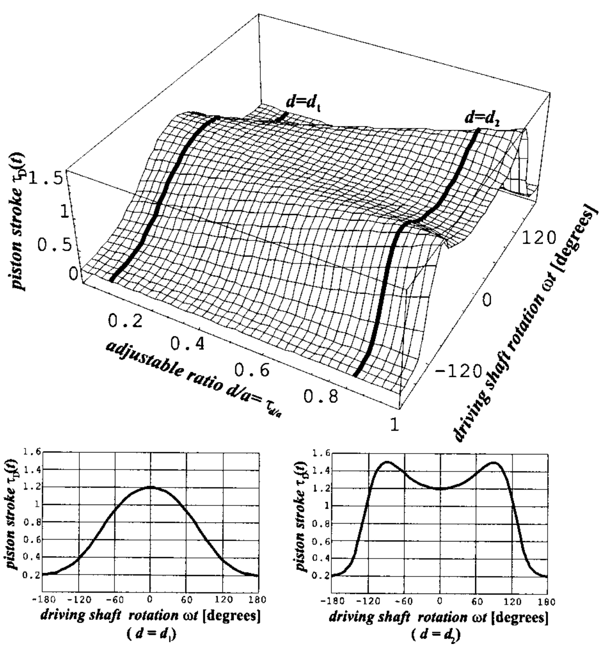

Fig. 3 Piston D position as function of the drive shaft rotation angle and of the variable distance *d*

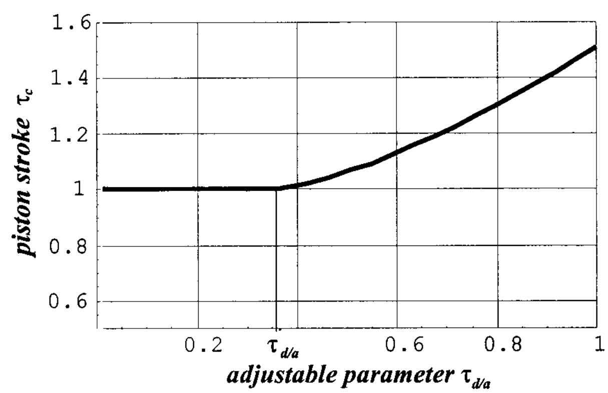

Fig. 4 Piston stroke as a function of the adjustable distance ratio $\tau_{d/a}$

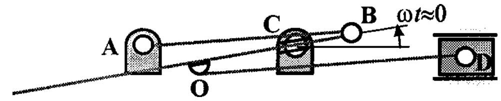

Fig. 5 Rods position when $t \approx 0$

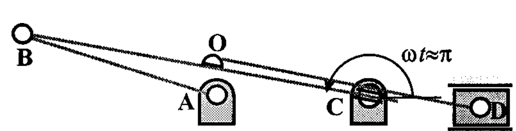

Fig. 6 Rods position when $\omega t \approx \pi$

If the piston stroke diagram is observed, when the parameter $\tau_{d/a}$ changes (as shown in Fig. 4), it is possible to conclude that:

- if $\tau_{d/a} < \tau^*_{d/a}$, the stroke doesn't change with $\tau_{d/a}$, but it keeps a constant value;
- if $\tau_{d/a} > \tau^*_{d/a}$, the maximum displacement of piston D changes roughly proportionally to $\tau_{d/a}$, as required by the applications.

If $\tau_{d/a} < \tau^*_{d/a}$, the piston displacement has its maximum value when $\omega t = 0$ (condition represented in Fig. 5) and its minimum is worth $\omega t = \pi$ (situation of Fig. 6); when $\omega t = 0$:

$$\tau_{\mathrm{D}}(0) = 1 - \tau_{r/a} + \tau_{b/a} \tag{11}$$

while, if $\omega t = \pi$.

$$\tau_{\mathrm{D}}(\pi/\omega) = -1 + \tau_{r/a} + \tau_{b/a} \tag{12}$$

then it results that the piston stroke is given by:

$$\tau_c = 2(1 - \tau_{r/a}) \tag{13}$$

and it is independent from the variable distance *d*.

Then, to apply the studied crank mechanism to control the piston stroke, a particular configuration of the mechanism is needed: for each value of length *d*, the second condition explained ($\tau_{d/a} > \tau^*_{d/a}$) must be verified. The piston runs two complete strokes for each rotation of the drive shaft, it presents two symmetric maximums and two minimum values when $\omega t = 0$ and $\omega t = \pi$.

Conditions on Rod Lengths

In Fig. 7 the diagram of piston displacement extreme positions are represented; the bifurcation corresponds to value $\tau^*_{d/a}$ of parameter $\tau_{d/a}$: the origin, that is the maximum point when $\tau_{d/a} < \tau^*_{d/a}$, becomes a relative minimum point when $\tau_{d/a} = \tau^*_{d/a}$ and the second derivative of function $\tau_{\mathrm{D}}(t)$ must assume value zero.

Analytically, it gives:

$$\left[\frac{d^2\tau_{\mathrm{D}}(t)}{dt^2}\right]_{t=0} = 0 \Leftrightarrow -1 - 2\tau^*_{d/a} - (\tau^*_{d/a})^2 + \tau_{r/a} - \frac{(1 - \tau^*_{d/a} - \tau_{r/a})^2}{\tau_{b/a}} = 0 \tag{14}$$

To impose in equation (14) that $\tau_{d/a} > \tau^*_{d/a}$ for each value of $\tau_{d/a}$, it is required that $\tau^*_{d/a} = 0$; then, the following condition referred to rod length is obtained:

$$-1 + \tau_{r/a} - \frac{(1 - \tau_{r/a})^2}{\tau_{b/a}} = 0 \tag{15}$$

that gives the solution $\tau_{r/a} = 1$, that means lengths BO and AB must be equal.

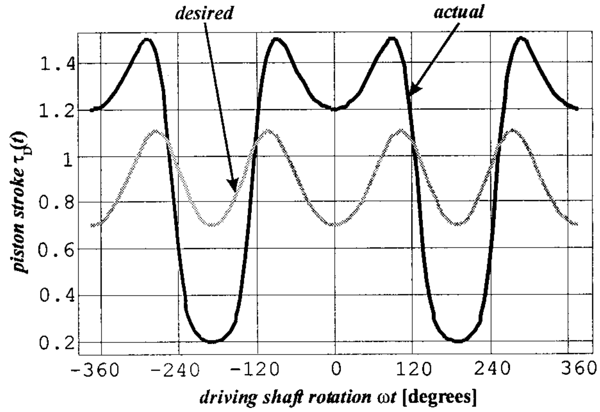

Fig. 8 Desired and actual piston displacement

This condition guarantees that time axis origin will be a minimum point, that the piston motion will include two strokes for each drive shaft rotation and that the piston stroke will change with the variable distance *d*, as required.

To enlarge the application fields of the system, two other conditions must be imposed on piston motion characteristics, in addition to the condition (15):

- both the two strokes of the piston for each drive shaft rotation must be complete;
- the two strokes must require the same time, to be considered equivalent.

The piston motion obtained with a general choice of rod lengths doesn't show the last two characteristics, as illustrated in Fig. 8.

From an analytical point of view, the first condition is equivalent to:

$$\tau_{\mathrm{D}}(0) = \tau_{\mathrm{D}}\left(\frac{\pi}{2}\right) \Leftrightarrow 2(1 - \tau_{r/a}) = 0 \tag{16}$$

Equation (16) is satisfied for each value of $\tau_{d/a}$ only if $\tau_{r/a} = 1$, that is only if lengths AB and BO are congruent; then, the new condition (16) doesn't add anything to the condition (15). The system behavior is represented in Fig. 9, as function of the drive shaft rotation angle and of the variable parameter $\tau_{d/a}$ when the condition (15) is respected.

On the contrary, the second condition indicated is the equivalent of imposing the presence of a maximum when the drive shaft rotation has the value $\pi/2$:

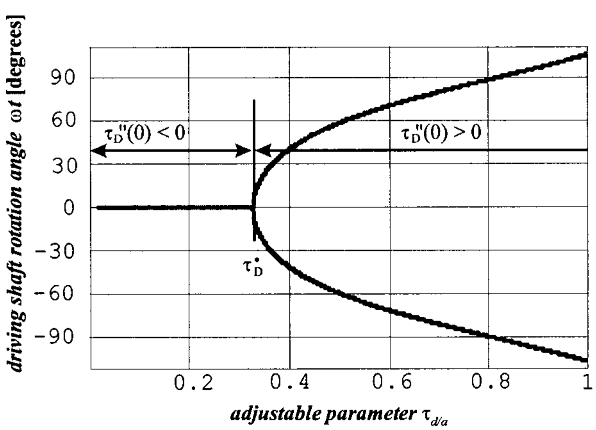

Fig. 7 Piston displacement extreme position set

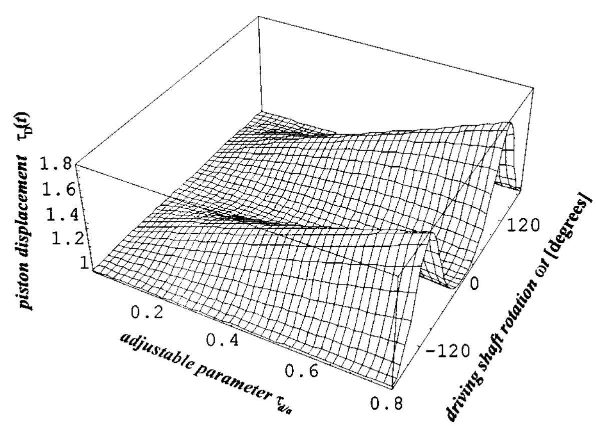

Fig. 9 Piston displacement versus shaft rotation and $\tau_{d/a}$

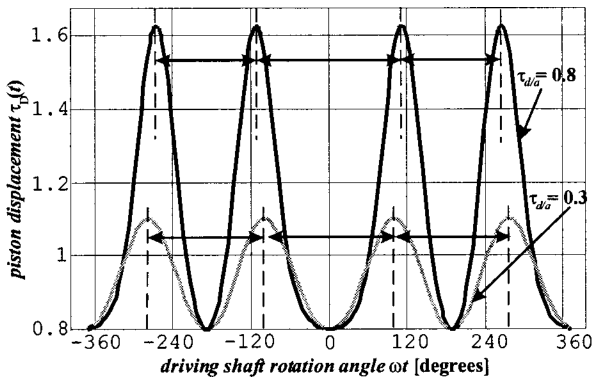

Fig. 10 Piston displacements for two values of the adjustable distance *d*

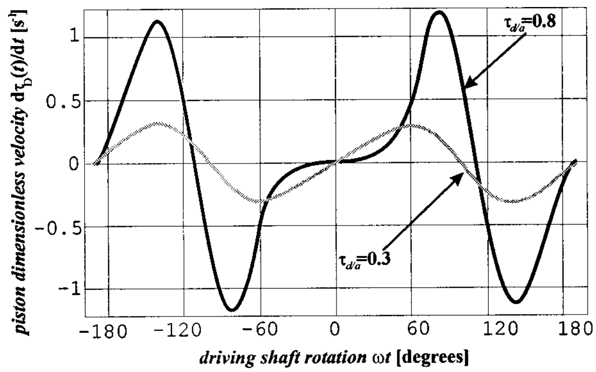

Fig. 12 Velocity of piston D versus shaft rotation

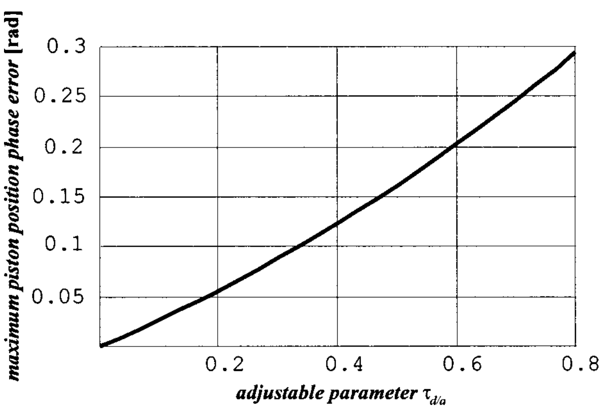

Fig. 11 Phase error versus $\tau_{d/}$

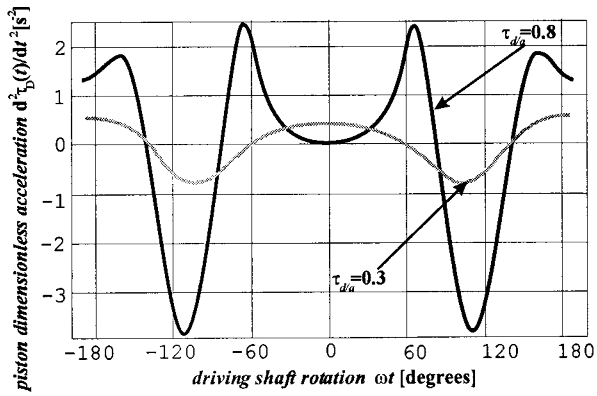

Fig. 13 Acceleration of piston D versus shaft rotation

$$\left[\frac{d\tau_D(t)}{dt}\right]_{\pi/2\omega}=0 \tag{17}$$

If we impose also that $\tau_{r/a}=1$, as obtained from Eqs. (15) and (16), the condition (17) can be analytically represented as:

$$1-\sqrt{1-\tau_{d/a}^2}-\frac{\tau_{d/a}(-1+\sqrt{1-\tau_{d/a}^2})}{\tau_{r/a}\sqrt{1-\frac{(-1+\sqrt{1-\tau_{d/a}^2})^2}{\tau_{r/a}^2}}}=0 \tag{18}$$

Unlike Eqs. (15) and (16), Eq. (18) does not allow a solution independent from the variable distance d, but it's satisfied only when $\tau_{d/a}=0$, that is when $d=0$.

This means that, if the two strokes of piston D must have an equal time length, a restriction on variation of the range of parameter d is needed.

In confirmation of what has been demonstrated, the diagrams of piston displacement obtained for two different values d are compared in Fig. 10 with $d=0.8\,a$ (that is $\tau_{d/a}=0.8$) and $d=0.3\,a$ (that is $\tau_{d/a}=0.3$); the graph obtained when $d=0.3\,a$ reproduces better the required characteristics for the piston motion.

Whereas, in Fig. 11, the diagram of the piston displacement phase error is illustrated as function of length d, between the driving shaft rotation angle value corresponding to the maximum point of piston displacement and its ideal value $-\pi/2$.

Piston Velocity and Acceleration

The following graphs represent the piston velocity (Fig. 12) and the piston acceleration (Fig. 13) when the condition (15) is verified and for two different values of distance d.

The diagrams confirm the previous remarks: if it is needed that the forward and backward motion of the piston during the first stroke has similar characteristics of that of the forward and backward motion during the second stroke, for every complete drive shaft rotation, it is necessary to limit the maximum variation of the stroke obtainable by the mechanism studied here, i.e. it is suitable to choose reduced values for the adjustable parameter $\tau_{d/a}$.

Conclusions

In the present paper the operating principles of a special mechanism have been shown, usable in order to vary the stroke length of the piston of a metering pump during its motion. Further the analytical kinematic model has been obtained. The system behavior has been studied under different ratios between the rods. The optimum design has been printed out to obtain the best working performance. In particular the noticeably different effects produced on the piston movement by different choice of the parameters are illustrated.

Nomenclature

a = rod AB length;
b = distance OD;
c = piston D stroke;
d = distance AC (adjustable);
$e(t)$ = distance BC;
$f(t)$ = distance OC;
r = radius BO;
t = time;
$x_D(t)$ = piston D position as a time function;

$\alpha(t)$ = rotation angle of rod AB;

$\delta(t)$ = rotation angle of the connecting rod (represented by the vector OD);

τ_c = c/a;

$\tau_{b/a}$ = ratio between the lengths b and a;

$\tau_{r/a}$ = ratio between the radius r and the length a;

$\tau_{d/a}$ = ratio between the lengths d and a;

$\tau_{d/a}^*$ = threshold value of $\tau_{d/a}$ that cause one or two piston strokes per shaft revolution;

$\tau_D(t)$ = $x_D(t)/a$.

$\tau_D^*(t)$ = value of $\tau_D(t)$ when $d/a=\tau_{d/a}^*$;

ω = drive shaft angular speed.

References

[1] Cambiaghi, D., and Mimmi, G., 1981, ''Studio di una Pompa Volumetrica Alternativa a Portata Variabile,'' Organi di trasmissione, No. **5**.

[2] Beyer, R., 1963, *Kinematics Synthesis of Mechanisms*, Chapman-Hall.

[3] Hein, K., 1967, *Applied Kinematics*, McGraw-Hill.

[4] Chironis, N. P., 1965, *Mechanisms, Linkages and Mechanical Controls*, McGraw-Hill.